Ammonium Addition (and Aerosol pH) has a Dramatic Impact on Volatility and Yield of Glyoxal SOA.

ARTICLE *in* ENVIRONMENTAL SCIENCE & TECHNOLOGY · DECEMBER 2013

Impact Factor: 5.33 · DOI: 10.1021/es4035667 · Source: PubMed

6 AUTHORS, INCLUDING:

Silja A. K. Häkkinen
University of Helsinki
16 PUBLICATIONS **272** CITATIONS
SEE PROFILE

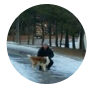

Yong Bin Lim
Korea Institute of Science and Technology
27 PUBLICATIONS **1,049** CITATIONS
SEE PROFILE

V. Faye Mcneill
Columbia University
68 PUBLICATIONS **1,044** CITATIONS
SEE PROFILE

Environmental Science & Technology

Article

pubs.acs.org/est

Ammonium Addition (and Aerosol pH) Has a Dramatic Impact on the Volatility and Yield of Glyoxal Secondary Organic Aerosol

Diana L. Ortiz-Montalvo,[†,⊥] Silja A. K. Häkkinen,[‡,§] Allison N. Schwier,[‡,∥] Yong B. Lim,[†] V. Faye McNeill,[‡] and Barbara J. Turpin*[,†]

[†]Department of Environmental Sciences, Rutgers University, New Brunswick, New Jersey 08901, United States

[‡]Department of Chemical Engineering, Columbia University, New York, New York 10027, United States

[§]Department of Physics, University of Helsinki, Helsinki 00560, Finland

Supporting Information

ABSTRACT: Glyoxal is an important precursor to secondary organic aerosol (SOA) formed through aqueous chemistry in clouds, fogs, and wet aerosols, yet the gas-particle partitioning of the resulting mixture is not well understood. This work characterizes the volatility behavior of the glyoxal precursor/product mix formed after aqueous hydroxyl radical oxidation and droplet evaporation under cloud-relevant conditions for 10 min, thus aiding the prediction of SOA via this pathway (SOA_{Cld}). This work uses kinetic modeling for droplet composition, droplet evaporation experiments and temperature-programmed desorption aerosol–chemical ionization mass spectrometer analysis of gas-particle partitioning. An effective vapor pressure ($p'_{L,eff}$) of ~10^{-7} atm and an enthalpy of vaporization ($\Delta H_{vap,eff}$) of ~70 kJ/mol were estimated for this mixture. These estimates are similar to those of oxalic acid, which is a major product. Addition of ammonium until the pH reached 7 (with ammonium hydroxide) reduced the $p'_{L,eff}$ to <10^{-9} atm and increased the $\Delta H_{vap,eff}$ to >80 kJ/mol, at least in part via the formation of ammonium oxalate. pH 7 samples behaved like ammonium oxalate, which has a vapor pressure of ~10^{-11} atm. We conclude that ammonium addition has a large effect on the gas-particle partitioning of the mixture, substantially enhancing the yield of SOA_{Cld} from glyoxal.

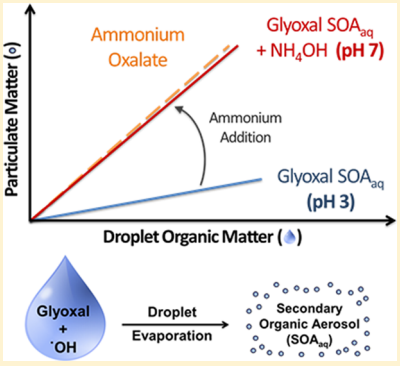

INTRODUCTION

Atmospheric aerosol affects the environment, climate, and human health.[1−3] However, our poor understanding of organic aerosol formed in the atmosphere [secondary organic aerosol (SOA)] hampers the ability of models to predict the magnitude, dynamics, and distribution of atmospheric aerosol from particle and precursor emissions.[4,5] Glyoxal (Gly), a small dicarbonyl ($C_2H_2O_2$), is perhaps the best-studied precursor of SOA formation through atmospheric aqueous chemistry (SOA_{aq}).[6,7] Gly is formed through gas phase oxidation of alkenes (e.g., isoprene and acetylene) and aromatics (e.g., benzene, toluene, and xylene).[8] It can also be emitted directly into the atmosphere by biomass burning[9] and the open ocean.[10] Gly partitions into atmospheric waters because of its high water solubility (Henry's law constant of 3.5 × 10^5 M/atm).[11] Once dissolved in the aqueous phase, Gly reacts through radical and nonradical reactions to form highly oxidized and less volatile compounds that remain at least partially in the particle phase after water evaporation.[6] Despite the attention that glyoxal SOA_{aq} has received, the gas-particle partitioning of the glyoxal precursor/product mixture is not well understood.

In cloudwater, the production of organic acids (e.g., oxalic acid) by OH radical oxidation of Gly is favored.[12] In contrast, in wet aerosols, OH radical oxidation of Gly and radical–radical reactions lead to the production of higher-molecular weight oligomeric products,[13] and reactions with inorganics present at high concentrations (e.g., ammonium) occur as well, forming, for example, nitrogen-containing organics such as imidazoles.[14] Chemistry can also take place during cloud droplet evaporation. Gly in evaporating droplets is known to form oligomers through self-reactions[15] and nitrogen-containing organics through reactions with amino acids[16] and amines.[17]

Despite advances in understanding the atmospheric aqueous chemistry of Gly, the volatility of the resulting precursor/product mixture has not been determined, to the best of our knowledge. This understanding is needed to predict the atmospheric gas-particle partitioning of this mixture and therefore glyoxal's SOA forming potential. We previously reported the effective vapor pressure and enthalpy of vaporization values for glycolaldehyde SOA_{aq}.[18] The goal of this work is to better characterize the volatility of the aqueous Gly + •OH precursor/product mix to improve the prediction of Gly SOA formed through cloud processing (SOA_{Cld}).

Received: August 10, 2013
Revised: December 7, 2013
Accepted: December 13, 2013
Published: December 13, 2013

In this work, we studied the volatility of the precursor/product mix formed via aqueous •OH oxidation of glyoxal under cloud-relevant conditions for 10 min. Using kinetic modeling to determine the droplet composition, droplet evaporation experiments, and temperature-programmed desorption aerosol−chemical ionization mass spectrometry (TPD aerosol−CIMS) analyses, we have provided, for the first time, estimates of fundamental physicochemical properties (vapor pressure and enthalpy of vaporization) for this mixture, which includes Gly, its oxidation products, and any additional chemistry that occurs in the evaporating droplets (e.g., oligomer formation). Importantly, this work also includes the first evaluation of the influence of ammonium hydroxide (e.g., neutralization, pH 7) on the volatility of SOA_{aq} mixtures. Ammonium addition has a substantial impact on the gas-particle partitioning of the product mixture, reducing the effective vapor pressure and increasing the yield of glyoxal SOA_{Cld}.

EXPERIMENTAL PROCEDURES

The (precursor + product) composition resulting from aqueous •OH oxidation of Gly under cloud-relevant conditions for 10 min was first determined via kinetic modeling, using a chemical model that has been validated against laboratory experiments.[12,13,19] Two atmospheric assumptions were evaluated: (1) depletion of Gly in the droplet (batch reactor) and (2) continuous replenishment of Gly in the droplet [continuously stirred tank reactor (CSTR)]. Because Gly has many sources, the more appropriate scenario might depend on location. Solutions were prepared with these compositions and used in droplet evaporation experiments that mimicked the evaporation of droplets after a single cloud processing cycle. Modeling was used, rather than •OH oxidation experiments, because experimental solutions would not have been chemically stable. Specifically, H_2O_2 photolysis is used to produce •OH in aqueous chemistry experiments. When aliquots of the sample were removed from the reaction vessel, catalase was typically added to prevent excess H_2O_2 from reacting with glyoxylic acid, a major product.[20] However, catalase is incompatible with the experimental apparatus we used for droplet evaporation. Thus, we avoided this problem by using mimic solutions (whose composition was determined by chemical modeling) for droplet evaporation experiments. Cloud droplet evaporation was simulated in the laboratory by means of a vibrating orifice aerosol generator (VOAG).[18] The volatility behavior of the Gly + •OH precursor/product mixture (representing the material present after one cloud cycle) was determined by comparing its behavior in the VOAG system with that of organic standards. The volatility behavior of mimic solutions was also studied with TPD aerosol−CIMS as described below.

Kinetic Modeling. The chemical model used to determine the composition of a cloud droplet exposed to Gly and •OH after one cloud processing cycle (10 min) is documented in the Supporting Information of ref 13. Two limiting cases were modeled. In the first scenario, the system is approximated by a batch chemical reactor and assumes that the gas phase production of Gly is slow compared to its aqueous oxidation. Thus, Gly in the cloud droplet is depleted as it reacts with •OH. The initial aqueous phase concentration of Gly in the batch model was 5 μM, which is within the concentration range found in cloudwater (<0.15−27 μM).[21] The concentration of aqueous phase •OH was held constant at 2.44×10^{-12} M, a value maintained by Henry's law equilibrium with gas phase •OH (H = 30 M/atm, 2×10^6 molecules of •OH/cm^3 in the gas phase).[13] This is consistent with estimated atmospheric concentrations in clouds (~10^{-12} to 10^{-13} M).[6]

In the second scenario, the system is treated as a CSTR, and thus, Gly is continuously replenished by the uptake of glyoxal into the droplet from the gas phase (CSTR). This would be the appropriate approximation if gas phase production were fast compared to aqueous oxidation. For CSTR modeling, the concentration of Gly was held constant at a cloud-relevant concentration of 5 μM. This is the equivalent of a Gly gas phase concentration of 0.014 ppb at Henry's law equilibrium, i.e., using a Henry's law constant equal to 3.5×10^5 M/atm.[11] As in the batch model runs, the •OH concentration in the aqueous phase was kept constant at 2.44×10^{-12} M. The chemical compositions of the Gly + •OH precursor/product mixture after aqueous oxidation for 10 min obtained from these two model runs (Figure 1) were used to prepare representative mimic solutions that were then analyzed through droplet evaporation experiments.

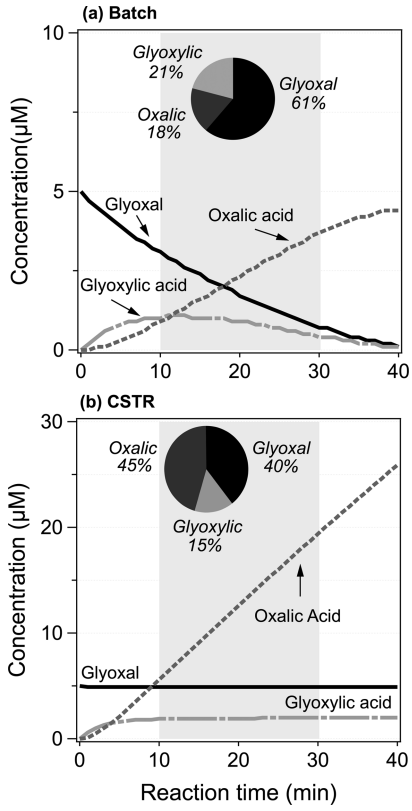

Figure 1. Estimated product concentrations for the reaction between 5 μM glyoxal and •OH (10^{-12} M), obtained from batch (a) and CSTR (b) assumptions. Pie charts illustrate the (molar) distribution of products 10 min into the reaction. Shaded areas between 10 and 30 min represent cloud droplet lifetimes.[41,42]

Mimic Samples. The following organic standards were used to prepare mimic solutions: glyoxal [39.7% (Sigma-Aldrich)], oxalic acid [0.1008 N (Fluka Analytical)], and glyoxylic acid [51.7% (Aldrich)]. Mimic solutions were prepared by diluting mixtures of organic standards with 18 MΩ milli-Q water. Concentrations were scaled up (F = 150 for CSTR, and F = 350 for batch) to allow the preparation of dilutions from approximately 500 to 4000 μM C, all above the detection limits of the droplet evaporation system, while the same distribution

of species was maintained. (Note the least concentrated of these dilutions is a fog-relevant concentration.) Additionally, ammonium hydroxide [29.6% as ammonia (NH_3) (J. T. Baker)] was used to increase the pH of CSTR mimics to study the effect of neutralization (pH 7).

Assessment of Volatility Using Droplet Evaporation Experiments. The methodology used for droplet evaporation and volatility assessment was described in detail by Ortiz-Montalvo et al.,[18] who used this approach to study the volatility of glycolaldehyde SOA. (Note that in the previous work the effect of neutralization on volatility was not studied.) Briefly, six dilutions (0–4000 μM C) of each mimic solution and several organic standards [acetic, oxalic, succinic, glutaric, and tartaric acids and ammonium oxalate (99.0%) (Fluka Analytical)] were pushed through a VOAG (TSI model 3450);[22] the resulting monodisperse droplets were dried to a relative humidity (RH) of ~10%, and their dry diameter was measured with an optical particle counter (OPC, Grimm Aerosol Spectrometer, model 1.109, 31 channels). Additionally, each mimic solution was analyzed for total organic carbon (TOC) (Shimadzu model TOC-5000A). The organic matter in each droplet ($OM_{droplet}$) was calculated from the TOC content using ratios of organic molecular weight to carbon weight [OM/OC (Table S1 of the Supporting Information)]. The residual optical particle diameters (D_p) measured by the OPC were converted to the mass of residual particles (PM mass) by assuming spherical particles and using liquid densities (Table S1 of the Supporting Information). Then the PM mass of each organic standard was regressed linearly on OM mass as shown in Figure 2 (slopes in Table S2 of the Supporting Information), and the slopes [PM mass/OM $mass_{(droplet)}$] were evaluated against their corresponding liquid vapor pressures ($p°_L$) (estimated using the SIMPOL group contribution method[23] and in the case of ammonium oxalate using the EPA-EPI suite[24]). Sigmoidal fits were obtained (Figure 3) because PM mass divided by droplet

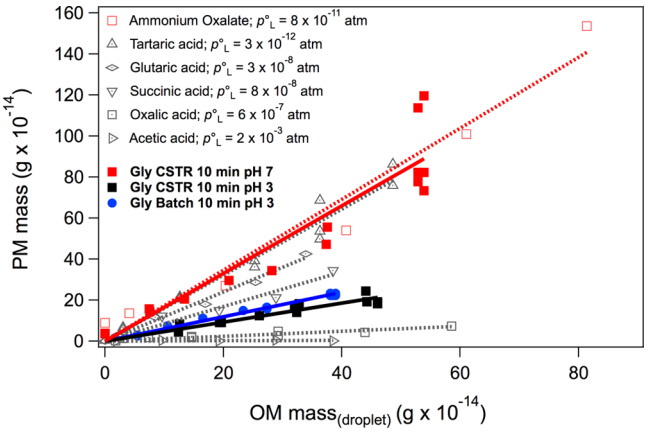

Figure 2. Residual PM mass vs initial droplet OM mass obtained from VOAG and TOC analyses, respectively. Filled red squares and the solid red line represent data for the Gly CSTR mimic at pH 7, while filled black squares and the solid black line correspond to data at pH 3. Filled blue circles and the solid blue line represent data for the Gly batch mimic at pH 3. Gray symbols and gray dashed lines represent data from organic acid standards. The legend includes estimates of liquid vapor pressure ($p°_L$) obtained from ref 23 for the organic acids and from the EPA-EPI suite[24] for ammonium oxalate (subcooled $p°_L$). Data for ammonium oxalate (empty red squares and dashed red line) are also shown. Samples were analyzed at a RH of 12 ± 3% and 24.4 ± 0.7 °C. Slopes and r^2 values are listed in Table 1.

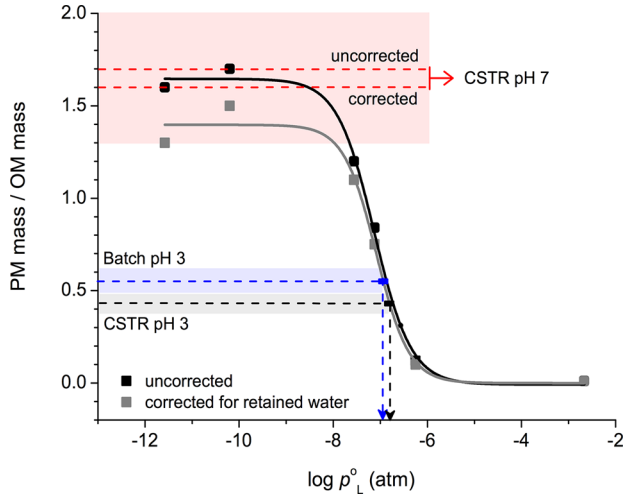

Figure 3. Sigmoidal fit of PM mass/OM mass vs log $p°_L$. PM mass/OM mass values correspond to slopes from Figure 2. Data shown were uncorrected (solid black line) and corrected (solid gray line) for the effect that retained water (33% upper-bound estimate) could have on PM density. Dashed lines show PM mass/OM mass values of Gly + •OH mimics and estimated $p°_L$ values from the corrected sigmoidal curve: black for CSTR at pH 3, blue for batch at pH 3, and red for CSTR at pH 7 (both corrected and uncorrected slope values are shown). Shaded areas represent the standard error of the slopes. The liquid vapor pressures of pure compounds ($p°_L$) were obtained from ref 23 for the organic acids and from the EPA-EPI suite[24] for ammonium oxalate (subcooled $p°_L$). PM mass/OM mass values are listed in Table 1 for Gly mimics and in Table S2 of the Supporting Information for the organic standards. The sigmoidal corrected regression equation can be found in Table S3 of the Supporting Information.

OM mass [ΔPM mass/ΔOM $mass_{(droplet)}$ = slope] reflects the fraction of total droplet OM that remains in the particle phase (i.e., particle fraction). Similarly, the slopes of the organic acid standards were also evaluated against their corresponding enthalpies of vaporization [estimated using a group contribution method that uses the normal boiling point to estimate the enthalpy of vaporization of pure compounds[25] (Figure S1 of the Supporting Information)]. Note that ammonium oxalate was not included in the sigmoidal regression of enthalpy of vaporization because of a lack of experimental and predictive values. As detailed by Ortiz-Montalvo et al.,[18] curves are also shown with a correction to account for the maximal effect that residual water could have on particle density, based on the fact that some organic compounds, like tartaric acid, retain water even at a RH as low as 5%.[26] The effective liquid vapor pressure ($p'_{L,eff}$) and the enthalpy of vaporization ($\Delta H_{vap,eff}$) of the droplet Gly + •OH precursor/product mix were estimated from these sigmoidal curves and PM mass/OM $mass_{(droplet)}$ of the Gly + •OH mimics. The correlations between PM mass and OM mass for mimic dilutions were high [r^2 > 89% (Table 1)], suggesting the volatility behavior was independent of the initial concentration.

In this work, the VOAG[22] system was operated as follows. Filtered mimic solutions (or organic standards) were passed through a 10 μm diameter (nominal ±25%) VOAG orifice, generating monodisperse droplets (20 μm nominal diameter). A drying chamber (6 s residence time) then was used for the evaporation of the droplets, and the diameter of the resulting particles at 12 ± 3% RH and 24.4 ± 0.7 °C was measured with the OPC downstream of a ^{210}Po ionizer (NRD StaticMaster;

dx.doi.org/10.1021/es4035667 | Environ. Sci. Technol. 2014, 48, 255–262

Table 1. VOAG Results for Gly + •OH Precursor/Product Mixtures, Including Slopes [PM mass/OM mass$_{(droplet)}$] with Coefficients of Determination (r^2) and Standard Errors, Effective Liquid Vapor Pressures ($p'_{L,eff}$), and Effective Enthalpies of Vaporization ($\Delta H_{vap,eff}$)

mimic sample	pH	density[a] (g/mL)	slope[b]	standard error	r^2 (%)	$p'_{L,eff}$[c] (atm)	$\Delta H_{vap,eff}$[d] (kJ/mol)	theoretical $\Delta H_{vap,mix}$[e] (kJ/mol)
batch for 10 min	3	1.3	0.55[f]	0.06	99	$(1 \pm 1) \times 10^{-7}$ [f]	70 ± 2[f]	44
CSTR for 10 min	3	1.4	0.43[g]	0.05	95	$(2 \pm 2) \times 10^{-7}$ [g]	70 ± 2[g]	54
	7	1.4−1.5[h]	1.6[i]	0.3	89	$<10^{-9}$ [j]	>80[j]	–

[a]Concentration-weighted density[39] ± 0.1 (error propagation accounting for the uncertainty in the concentrations) (Table S1 of the Supporting Information). [b]Slopes from Figure 2 corrected for the effect that retained water (33% upper-bound estimate) could have on the density value used to calculate PM mass. Slopes for organic standards are listed in Table S2 of the Supporting Information. [c]Effective liquid vapor pressure estimates (at 298.15 K) using the corrected sigmoidal regression shown in Figure 3 ± error propagation, which incorporates the uncertainty in vapor pressure estimates,[23] the standard error of the slope, and the standard error in the coefficients of the sigmoidal regression. The sigmoidal corrected regression equation can be found in Table S3 of the Supporting Information. [d]Effective enthalpy of vaporization estimates (at normal boiling point) using corrected sigmoidal regression shown in Figure S1 of the Supporting Information ± error propagation, which incorporates the uncertainty in the enthalpy of vaporization estimates,[25] the standard error of the slope, and the standard error in the coefficients of the sigmoidal regression. The sigmoidal corrected regression equation can be found in Table S4 of the Supporting Information. [e]Molar-weighted theoretical enthalpies of vaporization of product mixtures calculated following the method of Chickos et al.,[38] as $\Delta H_{vap,mix} = \sum_i n_i \times \Delta H_{vap,i}$, where n_i is the molar fraction of species i (from Figure 1) and $\Delta H_{vap,i}$ is the theoretical enthalpy of vaporization of species i (33.486, 72.57, and 50.191 kJ/mol for glyoxal, oxalic acid, and glyoxylic acid, respectively, at the normal boiling point).[30] [f]A sensitivity analysis using the density of solid glyoxal trimer dihydrate to calculate the density of the mixture (Table S1 of the Supporting Information) resulted in an increase in the slope (0.60) and $\Delta H_{vap,eff}$ (71 ± 2 kJ/mol), but $p'_{L,eff}$ remained unchanged. [g]Sensitivity analysis using the density of solid glyoxal trimer dihydrate (Table S1 of the Supporting Information) resulted in an increase in the slope (0.46), a decrease in $p'_{L,eff}$ to $(1 \pm 2) \times 10^{-7}$ atm, and no change in $\Delta H_{vap,eff}$. [h]Assuming a density between that of the CSTR for 10 min at pH 3 and ammonium oxalate (1.50 g/mL).[40] [i]The slope without correction for retained water was 1.7 ± 0.3. [j]Estimated on the basis of the uncorrected sigmoidal regression. Note that CSTR pH 7 mimic behaved like ammonium oxalate, which has a vapor pressure on the order of 10^{-11} atm.[24]

gives particles a Boltzmann charge distribution). The particle residence time (6 s) is longer than typical times used to equilibrate ambient particles in aerosol hygroscopicity studies using tandem differential mobility analyzer measurements and is considered to be sufficiently long for water equilibration (assuming an accommodation coefficient of 0.02).[27] The diameter of the generated droplets was determined by calibrating the system with ammonium sulfate [3.1801 M $(NH_4)_2SO_4$ (Fluka Analytical)]. The droplet diameter (D_d = 17.60 ± 0.03 μm, n = 2, r^2 = 0.99) was obtained from the slope of D_p versus $C^{1/3}$, where D_p is the residual particle diameter and C the volumetric concentration of the solute in solution ($cm^3_{solute}/cm^3_{solution}$). The D_p of mimic samples ranged between 0.36 and 1.16 μm, with geometric standard deviations between 1.1 and 1.4. The VOAG system was operated at a frequency of ∼160 kHz, a liquid flow rate of 0.077 mL/min, dilution air of 50 L/min, and dispersion air of 1 L/min.

The performance of the VOAG system was tested daily by sampling (in duplicate) standard solutions of 250 μM $(NH_4)_2SO_4$ and using the criterion for acceptance of a 10% (or less) difference between the measured particle diameter of $(NH_4)_2SO_4$ and the theoretical one. Succinic acid standards [99.99% (Sigma-Aldrich)] were used as an independent check. Samples of 60 and 750 μM succinic acid (n = 10 each) were analyzed in duplicate during each experiment, and a method precision for the diameter was obtained (2 and 1%, respectively, expressed as pooled coefficients of variation). To test the accuracy of the volatility assessment, malonic acid standard solutions [six dilutions between 0 and 3000 μM C from 0.999% (Sigma-Aldrich)] were sampled just like the mimic solutions. The estimated $p'_{L,eff}$ for malonic acid [$(6 \pm 7) \times 10^{-8}$ atm] was within 1 order of magnitude of the calculated theoretical value [$(2 \pm 2) \times 10^{-7}$ atm; SIMPOL group contribution method].[23] The estimated $\Delta H_{vap,eff}$ (72 ± 2 kJ/mol) was within 5% of the theoretical value (69 ± 2 kJ/mol; Joback and Reid group contribution method).[25] We note that an additional uncertainty (∼17%) might be introduced by differences in the refractive index between malonic acid (1.479) and polystyrene latex particles (1.59), which were used to make the OPC manufacturer-supplied calibration.

TPD Aerosol−CIMS Measurements. Bulk CSTR mimic solutions were also analyzed by TPD aerosol−CIMS to examine volatility behavior. Bulk mimic solutions were aerosolized with N_2 using a constant output atomizer (TSI 3076; operated at a rate of 2.2−2.5 L/min). This wet aerosol passed through a diffusion dryer and was combined with a dry N_2 dilution flow (2.6−3.0 L/min) to keep the RH of the aerosol stream below 12%. A portion of the flow (1.8 L/min, maintained by a critical orifice) entered a volatilization flow tube (residence time of <1 s; 23 cm long, 1.08 cm inside diameter stainless steel tube wrapped in heating tape with a thermocouple and temperature controller). There the aerosol was introduced at temperatures ranging between 25 and 160 °C to volatilize the organics for gas phase detection by CIMS. The total residence time between atomization and the CIMS entrance was 6 s. Another portion of the flow (0.3 L/min) was characterized using a scanning mobility particle sizer (TSI). The remaining flow was exhausted. The generated aerosol had a log-normal number size distribution with a geometric mean particle diameter of 32 ± 3 nm and geometric standard deviation of 1.6. Directly after the volatilization region, the aerosol entered the chemical ionization region of the mass spectrometer. CIMS measurements were taken in negative detection mode using I^- reagent ions, generated by passing N_2 at a rate of 2.5 L/min over a permeation tube of CH_3I held at 52 °C and sending it through a ^{210}Po ionizer (NRD) into the chemical ionization region of the aerosol−CIMS. Details of the design and operation of the CIMS instrument can be found in ref 28.

Volatilization studies using TPD aerosol−CIMS were conducted by tracing the mass-to-charge ratios (m/z) of the detectable organics and evaluating how the signal responded to changes in temperature[29] (i.e., 25−160 °C). A full mass spectrum was first determined on each mimic sample to verify

that the species could be detected in the gas phase in negative detection mode. Oxalic acid appears at m/z 217 as $I^-{\cdot}C_2H_2O_4$; glyoxal was detected in its hydrated form at m/z 203 ($I^-{\cdot}C_2H_4O_3$), and glyoxylic acid was detected at m/z 201 ($I^-{\cdot}C_2H_2O_3$). Each mimic solution was analyzed at least twice. A solution of 1 mM oxalic acid standard was also analyzed; its measured $\Delta H_{vap,eff}$ (85 ± 12 kJ/mol) was within 10−12% of the theoretical value (94−97 kJ/mol),[30] over a temperature range of 25−56 °C. $\Delta H_{vap,eff}$ was calculated using the Clausius−Clapeyron relation, as explained in section S1 of the Supporting Information.

RESULTS AND DISCUSSION

After aqueous •OH (~10^{-12} M) oxidation of glyoxal (5 μM) for 10 min, the major species are oxalic acid, glyoxylic acid, and unreacted glyoxal (Figure 1). Glyoxal is the greatest contributor in the batch scenario; oxalic acid is greatest in the CSTR scenario (pie charts in Figure 1). Glyoxal is known to self-oligomerize upon droplet evaporation;[15,31] hence, some portion of the glyoxal is expected to contribute to residual PM (Gly SOA_{Cld}). Although oxalic acid has an intermediate volatility (~10^{-7} atm),[18] field measurements indicate that oxalate is found in the atmosphere mostly in the particle phase.[32] We suspect this is because oxalate is frequently present as a salt (e.g., ammonium oxalate); the vapor pressure of ammonium oxalate is orders of magnitude lower than that of oxalic acid. Also, ammonium might plausibly react with glyoxal during droplet evaporation. Therefore, we expect that the addition of ammonium hydroxide to our 10 min mimic samples will lower the vapor pressure of the mimics. In this work, we confirm that the addition of ammonium to the CSTR Gly + •OH precursor/product mix lowers the vapor pressure of the sample and argue that acid−base neutralization has the potential to explain this effect; other mechanisms could also contribute.

The addition of ammonium to the Gly + •OH mimic (CSTR) significantly increased the level of retention of PM mass upon evaporation of droplet OM mass (Figure 2; pH 7 in solid red vs pH 3 in solid black). In Figure 2, the values of PM mass versus OM $mass_{(droplet)}$ of the mimics are compared with those of ammonium oxalate (empty red squares and dotted line) and organic acid standards (gray symbols and dotted lines). Note the compounds with the lowest liquid vapor pressures (see the legend) have the largest residual PM mass (e.g., tartaric acid and ammonium oxalate). The slope [PM mass/OM $mass_{(droplet)}$] of the linear regression is steepest for those compounds (Figure 2), indicating that a larger fraction of the organic mass is retained in the particle phase. Furthermore, the Gly + •OH mimic containing ammonium hydroxide (pH 7) (Figure 2, solid red line) exhibited behavior in the VOAG system similar to that of ammonium oxalate (dashed red line) and had a slope much larger than that of the ammonium-free mimic (Figure 2, solid black line). This suggests that the vapor pressure of the Gly + •OH precursor/product mixture decreases by orders of magnitude as a result of ammonium addition. The increase in the slope [PM mass/OM $mass_{(droplet)}$] from pH 3 to 7 was significant (Table 1; slopes of 0.43 ± 0.05 and 1.6 ± 0.3, respectively; two-sided t test, $p = 0.05$), resulting in an effective vapor pressure for the ammonium-containing mixture that was too low to be measured accurately in our system, as explained below.

The $p'_{L,eff}$ values of the pH 3 mimics (batch and CSTR) are both ~10^{-7} atm according to Figure 3. In Figure 3, the slopes [PM mass/OM $mass_{(droplet)}$] of the standards from Figure 2 (Table S2 of the Supporting Information) and their liquid vapor pressures were used to establish sigmoidal regressions and predict the effective vapor pressures of Gly + •OH mimics from their PM mass/OM $mass_{(droplet)}$ values, as illustrated by the corresponding arrows (black for CSTR at pH 3 and blue for batch at pH 3). $\Delta H_{vap,eff}$ values (~70 kJ/mol) were determined from a similar sigmoidal regression shown in Figure S1 of the Supporting Information. In Figure 3 and Figure S1 of the Supporting Information, two sigmoidal regressions are shown: one uncorrected (solid black line) and one corrected for the upper-bound effect of retained water on particle density (solid gray line) assuming that all standards retained as much water as observed for tartaric acid. Both curves provide identical results for the pH 3 mimics. Theoretical molar-weighted enthalpies of vaporization for the pH 3 mimics (see Table 1) are lower than the measured values. The difference between theoretical and VOAG-estimated enthalpies could be due to (1) products formed during droplet evaporation because these are not included in the theoretical calculations (e.g., glyoxal oligomers) and/or (2) residual water retained by the particles downstream of the VOAG, which would result in larger measured particle diameters and consequently larger PM mass/OM $mass_{(droplet)}$ ratios and higher enthalpy estimates. Thus, the measured values we report in Table 1 should be considered upper-bound estimates.

As shown in Figure 3, the neutralized (pH 7) Gly CSTR−SOA_{Cld} sample behaved as if it stayed entirely in the particle phase at ambient temperature (red dashed lines), much like ammonium oxalate and tartaric acid (first two points at the top left of the sigmoidal regressions). We are unable to provide accurate estimates of the volatility of the neutralized Gly + •OH mimic because the data for this sample fall within the part of the regression that is insensitive to vapor pressure (Figure 3) or enthalpy of vaporization (Figure S1 of the Supporting Information). This work suggests that the CSTR pH 7 mimic has an $p'_{L,eff}$ of <10^{-9} atm and a $\Delta H_{vap,eff}$ of >80 kJ/mol (Table 1). Note that pH 7 mimics behaved like ammonium oxalate, which has a vapor pressure on the order of 10^{-11} atm. More precise estimates of the volatility of the neutralized Gly + •OH precursor/product mixture could be obtained by conducting VOAG experiments at higher temperatures or lower pressures, shifting the sigmoidal regression to the left. Despite the current uncertainty in estimating the volatility of the neutralized Gly + •OH mimic, it is evident that the presence of ammonia in cloud droplets containing Gly and •OH will substantially reduce the vapor pressure of the mixture, causing it to behave like ammonium oxalate (~10^{-11} atm) and increasing the yield of in-cloud Gly SOA_{aq}. This result is consistent with the work of Na et al.,[33] who found that ammonia enhanced SOA formation from α-pinene ozonolysis because of the formation of condensable (organic) salts. These findings indicate that ammonia can play an important role in the properties and fate of SOA formed through cloud processing.

There are several competing mechanisms that could contribute to the enhancement of PM mass (and decrease in volatility) observed upon addition of ammonium hydroxide: salt formation from acid−base neutralization of organic acids by ammonia, equilibrium shifts caused by "salting in" of aerosol phase glyoxal by electrolytes[34] (i.e., ammonium salts), oligomer formation from glyoxal self-reactions catalyzed by ammonium ions[35] in evaporating droplets,[15] and formation of nitrogen-containing compounds from glyoxal + ammonia reactions.[14,35] Neutralization of oxalic acid by ammonia is sufficient to explain

dx.doi.org/10.1021/es4035667 | Environ. Sci. Technol. 2014, 48, 255−262

our results because (1) the PM mass/OM mass$_{(droplet)}$ ratios of the pH 7 mimic were in agreement with those of the ammonium oxalate standard (Figure 2) and (2) a substantial increase in PM mass was observed when ammonium hydroxide was added to a 1 mM standard solution of oxalic acid, and its PM mass/OM mass$_{(droplet)}$ ratio was equal to the ratio obtained for a 1 mM standard solution of ammonium oxalate (Figure S2 of the Supporting Information). However, contributions by other mechanisms (e.g., glyoxal + ammonia reactions) are certainly possible.

In the case of TPD aerosol–CIMS analysis, $\Delta H_{vap,eff}$ values were calculated for individual species detected in the mimics (in contrast to VOAG's $\Delta H_{vap,eff}$ values for the entire mimic mixture). CIMS results confirm that oxalate is less volatile in the ammonium-containing (pH 7) samples. Figure 4 shows the

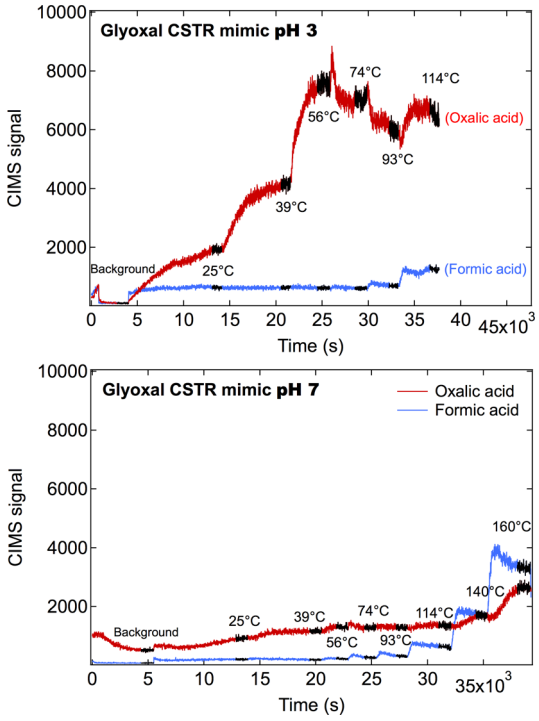

Figure 4. Oxalic and formic acid aerosol–CIMS signal as a function of time at different mean inlet temperatures. Representative data for the CSTR pH 3 mimic sample are shown in the top panel and data for the CSTR pH 7 mimic sample in the bottom panel. Data colored black correspond to the specified temperature. Panels are aligned at 114 °C to illustrate the high temperatures (≤160 °C) needed for oxalic acid in the CSTR pH 7 mimic to evaporate.

signal of oxalic acid (m/z 217, red) measured by CIMS in the gas phase as a function of time with increasing temperature, for both pH 3 (top panel) and pH 7 (bottom panel) CSTR mimics. Also shown in Figure 4 in blue is the signal of formic acid (m/z 173 as $I^-{\cdot}CH_2O_2$), a product of oxalic acid's thermal decomposition. The magnitude of the gas phase signal of oxalic acid in the pH 3 sample (top panel) was twice as high at room temperature (25 °C) as that of the signal for the pH 7 sample. The magnitude of the pH 3 oxalic acid signal continued to increase with an increase in temperature until thermal decomposition was observed (>74 °C). In contrast, the magnitude of the signal of oxalic acid at pH 7 (bottom panel) remained low, increasing only slightly above 114 °C, accompanied by decomposition to formic acid. The Clausius–Clapeyron relation (section S1 of the Supporting Information) indicates that the $\Delta H_{vap,eff}$ for oxalic acid in the pH 3 mixture (44 ± 5 kJ/mol) was lower than the theoretical ΔH_{vap} of pure oxalic acid in the temperature range of 25–114 °C (90–97 kJ/mol).[30] The decrease in $\Delta H_{vap,eff}$ for a compound in a mixture compared to the ΔH_{vap} of the pure compound is consistent with previous findings for organic acid and aldehyde mixtures of oleate[29] and α-pinene[36] ozonolysis products. We are unable to provide accurate estimates of $\Delta H_{vap,eff}$ for oxalate in the ammonium-containing (pH 7) sample because of the combined effects of evaporation and decomposition of oxalate into formic acid. However, these results verify that the oxalate within the mimic becomes essentially nonvolatile below 100 °C in the presence of ammonium (pH 7).

The TPD aerosol–CIMS measurements also provide strong evidence that ammonium addition changes the gas-particle partitioning behavior of glyoxal (Figure 5). Glyoxal in the pH 3

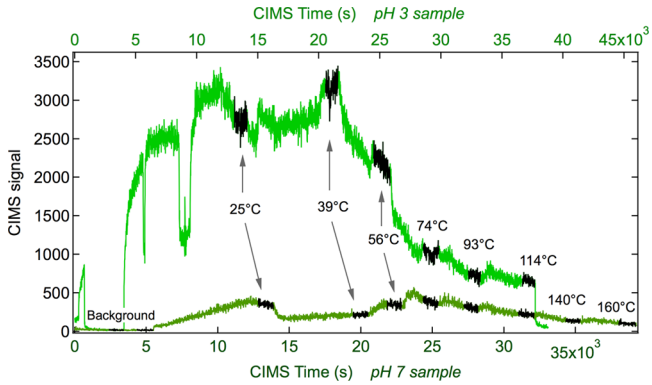

Figure 5. Aerosol–CIMS signal of glyoxal as a function of time at different mean inlet temperatures. Data from the CSTR pH 3 mimic are colored light green (top axis) and dark green for the pH 7 mimic (bottom axis). Data colored black correspond to the specified temperature.

mimic appears to be entirely in the gas phase at 25 °C, because its signal is strong and its magnitude does not increase with an increase in temperature (above 40 °C decomposition is evident). In contrast, the glyoxal signal from the pH 7 mimic is quite small at 25 °C, suggesting that interactions and/or reactions between ammonium and glyoxal are either stabilizing the glyoxal in the particle phase or leading to the formation of organic nitrogen products that we have not yet identified. No increase in the magnitude of the gaseous glyoxal signal is seen with an increase in temperature for the pH 7 mimic, suggesting that any glyoxal present remains in the particle phase or decomposes rather than volatilizing. Note that while we expect that the weaker glyoxal signal at high temperatures (pH 3) is a result of glyoxal decomposition, such a feature could also occur if the high temperatures in the volatilization flow tube were to drive in-particle chemistry, leading to lower-volatility (e.g., oligomeric) products. The increase in the level of formic acid at elevated temperatures (Figure 4) occurs as a result of oxalic acid decomposition in the thermodenuder. However, formic acid is a major product of glyoxal + ammonia reactions.[14] Thus, the observation that the formic acid/oxalic acid ratios at pH 3 and 7 are the same in the ambient-temperature aerosol–CIMS measurements (Figure 4) suggests that glyoxal + ammonia reactions are minor and do not explain the decrease in volatility of the mimics upon addition of ammonium hydroxide.

dx.doi.org/10.1021/es4035667 | Environ. Sci. Technol. 2014, 48, 255–262

In conclusion, we found that the volatility of Gly + •OH precursor/product mixture after cloud processing for 10 min was insensitive to the assumption made to model the droplet composition (i.e., whether gas phase glyoxal production was fast enough to replace reacting glyoxal in the aqueous phase). A significant decrease in the effective vapor pressure was observed when ammonium hydroxide was added to the 10 min Gly + •OH precursor/product mixture (pH 7). The pH 7 Gly + •OH mimic appeared to remain entirely in the particle phase at ambient temperature, as observed for the ammonium oxalate standard. Ammonium addition (e.g., through organic salt formation, salting in of glyoxal, reactions with glyoxal, and/or catalysis of oligomer formation)[14,34,35,37] has a large effect on the gas-particle partitioning of the Gly + •OH precursor/product mixture and therefore on the yield of glyoxal SOA_{Cld} (see yield comparisons in section S2 of the Supporting Information). These findings suggest that the gas-particle partitioning of the SOA_{Cld} mixture is highly dependent on the chemical form of the organic products (e.g., acid vs salt) and that glyoxal SOA_{Cld} could be an important source of SOA_{aq}, especially where and when ammonia levels are high.

■ ASSOCIATED CONTENT

Supporting Information

Organic mass to organic carbon ratios (OM/OC) and density values used to calculate OM mass and PM mass (Table S1), slopes (PM mass/OM mass ratios) obtained from linear regressions shown in Figure 2 (Table S2), sigmoidal regression of PM mass/OM mass versus log ΔH_{vap} (Figure S1), PM mass/OM mass ratios of 1 mM oxalate solutions (Figure S2), sigmoidal regression equation between corrected PM mass/OM $mass_{(droplet)}$ and log p°_{L} (Table S3), sigmoidal regression equation between corrected PM mass/OM $mass_{(droplet)}$ and log ΔH_{vap} (Table S4), examples of calculations of the effective enthalpy of vaporization estimates from the TPD aerosol–CIMS measurements (section S1), and SOA mass yields (section S2). This material is available free of charge via the Internet at http://pubs.acs.org.

■ AUTHOR INFORMATION

Corresponding Author

*E-mail: turpin@envsci.rutgers.edu. Phone: (848) 932-5781. Fax: (732) 932-8644.

Present Addresses

[‖]A.N.S.: Universite Blaise Pascal, Laboratoire de Meteorologie Physique, CNRS/OPGC, Clermont-Ferrand, France.

[⊥]D.L.O.-M.: National Institute of Standards and Technology, 100 Bureau Dr., Gaithersburg, MD 20899-8372.

Notes

The authors declare no competing financial interest.

■ ACKNOWLEDGMENTS

This research was supported, in part, by the Ford Foundation Dissertation Fellowship Award sponsored by the Ford Foundation and administered by the National Research Council of the National Academies and by the Mid-Atlantic States Section of the Air and Waste Management Association (MASS-A&WMA) Air Pollution Educational and Research Grant Program (APERG). This work was also supported by the GAANN (Graduate Assistance in Areas of National Need) Project P200A060156 Interdisciplinary Graduate Education in Environmental Science and Engineering (Grant NSF-ATM-0630298), NOAA (Grant NA07OAR4310279), EPA-STAR (RD-83375101-0), the New Jersey Agricultural Experiment Station, and USDA-NIFA. V.F.M. and A.N.S. acknowledge support of the NASA Tropospheric Chemistry program (Grant NNX09AF26G), and S.A.K.H. acknowledges a Fulbright Fellowship. Although the research described in this paper has been funded in part by the Environmental Protection Agency's STAR program, it has not been subjected to any Environmental Protection Agency (EPA) or other government agency review and therefore does not necessarily reflect the views of the EPA or any other government agency. No official endorsement should be inferred.

■ REFERENCES

(1) *Air Quality Criteria for Particulate Matter*; Environmental Protection Agency: Research Triangle Park, NC, 2004.

(2) *Particulate Matter Assessment for Policy Makers*; A NARSTO Assessment; McMurry, P., et al., Eds.; Cambridge University Press: Cambridge, U.K., 2004.

(3) IPCC. *Climate Change 2007: The Physical Science Basis*; Contribution of Working Group I to the Fourth Assessment Report of the Intergovernmental Panel on Climate Change (IPCC); Solomon, S., et al., Eds.; Cambridge University Press: Cambridge, U.K., 2007.

(4) Zhang, Q.; Jimenez, J. L.; Canagaratna, M. R.; Allan, J. D.; Coe, H.; Ulbrich, I.; Alfarra, M. R.; Takami, A.; Middlebrook, A. M.; Sun, Y. L.; Dzepina, K.; Dunlea, E.; Docherty, K.; DeCarlo, P. F.; Salcedo, D.; Onasch, T.; Jayne, J. T.; Miyoshi, T.; Shimono, A.; Hatakeyama, S.; Takegawa, N.; Kondo, Y.; Schneider, J.; Drewnick, F.; Borrmann, S.; Weimer, S.; Demerjian, K.; Williams, P.; Bower, K.; Bahreini, R.; Cottrell, L.; Griffin, R. J.; Rautiainen, J.; Sun, J. Y.; Zhang, Y. M.; Worsnop, D. R. Ubiquity and dominance of oxygenated species in organic aerosols in anthropogenically-influenced Northern Hemisphere midlatitudes. *Geophys. Res. Lett.* **2007**, *34*, L13801.

(5) Hallquist, M.; Wenger, J.; Baltensperger, U.; Rudich, Y.; Simpson, D.; Claeys, M.; Dommen, J.; Donahue, N.; George, C.; Goldstein, A. The formation, properties and impact of secondary organic aerosol: Current and emerging issues. *Atmos. Chem. Phys.* **2009**, *9*, 5155–5236.

(6) Ervens, B.; Turpin, B. J.; Weber, R. J. Secondary organic aerosol formation in cloud droplets and aqueous particles (aqSOA): A review of laboratory, field and model studies. *Atmos. Chem. Phys.* **2011**, *11*, 11069–11102.

(7) Blando, J. D.; Turpin, B. J. Secondary organic aerosol formation in cloud and fog droplets: A literature evaluation of plausibility. *Atmos. Environ.* **2000**, *34*, 1623–1632.

(8) Fu, T.-M.; Jacob, D. J.; Wittrock, F.; Burrows, J. P.; Vrekoussis, M.; Henze, D. K. Global budgets of atmospheric glyoxal and methylglyoxal, and implications for formation of secondary organic aerosols. *J. Geophys. Res.* **2008**, *113*, D15303.

(9) Hays, M. D.; Geron, C. D.; Linna, K. J.; Smith, N. D.; Schauer, J. J. Speciation of Gas-Phase and Fine Particle Emissions from Burning of Foliar Fuels. *Environ. Sci. Technol.* **2002**, *36*, 2281–2295.

(10) Sinreich, R.; Coburn, S.; Dix, B.; Volkamer, R. Ship-based detection of glyoxal over the remote tropical Pacific Ocean. *Atmos. Chem. Phys.* **2010**, *10*, 11359–11371.

(11) Betterton, E. A.; Hoffmann, M. R. Henry's law constants of some environmentally important aldehydes. *Environ. Sci. Technol.* **1988**, *22*, 1415–1418.

(12) Tan, Y.; Perri, M. J.; Seitzinger, S. P.; Turpin, B. J. Effects of precursor concentration and acidic sulfate in aqueous glyoxal–OH radical oxidation and implications for secondary organic aerosol. *Environ. Sci. Technol.* **2009**, *43*, 8105–8112.

(13) Lim, Y. B.; Tan, Y.; Perri, M. J.; Seitzinger, S. P.; Turpin, B. J. Aqueous chemistry and its role in secondary organic aerosol (SOA) formation. *Atmos. Chem. Phys.* **2010**, *10*, 10521–10539.

(14) Yu, G.; Bayer, A. R.; Galloway, M. M.; Korshavn, K. J.; Fry, C. G.; Keutsch, F. N. Glyoxal in aqueous ammonium sulfate solutions: Products, kinetics and hydration effects. *Environ. Sci. Technol.* **2011**, *45*, 6336–6342.

(15) De Haan, D. O.; Corrigan, A. L.; Tolbert, M. A.; Jimenez, J. L.; Wood, S. E.; Turley, J. J. Secondary organic aerosol formation by self-reactions of methylglyoxal and glyoxal in evaporating droplets. *Environ. Sci. Technol.* **2009**, *43*, 8184−8190.
(16) De Haan, D. O.; Corrigan, A. L.; Smith, K. W.; Stroik, D. R.; Turley, J. J.; Lee, F. E.; Tolbert, M. A.; Jimenez, J. L.; Cordova, K. E.; Ferrell, G. R. Secondary organic aerosol-forming reactions of glyoxal with amino acids. *Environ. Sci. Technol.* **2009**, *43*, 2818−2824.
(17) De Haan, D. O.; Tolbert, M. A.; Jimenez, J. L. Atmospheric condensed-phase reactions of glyoxal with methylamine. *Geophys. Res. Lett.* **2009**, *36*, DOI:10.1029/2009GL037441.
(18) Ortiz-Montalvo, D. L.; Lim, Y. B.; Perri, M. J.; Seitzinger, S. P.; Turpin, B. J. Volatility and yield of glycolaldehyde SOA formed through aqueous photochemistry and droplet evaporation. *Aerosol Sci. Technol.* **2012**, *46*, 1002−1014.
(19) Kirkland, J. R.; Lim, Y. B.; Tan, Y.; Altieri, K. E.; Turpin, B. J. Glyoxal secondary organic aerosol chemistry: Effects of dilute nitrate and ammonium and support for organic radical−radical oligomer formation. *Environ. Chem.* **2013**, *10*, 158−166.
(20) Tan, Y.; Carlton, A. G.; Seitzinger, S. P.; Turpin, B. J. SOA from methylglyoxal in clouds and wet aerosols: Measurement and prediction of key products. *Atmos. Environ.* **2010**, *44*, 5218−5226.
(21) Munger, J. W.; Jacob, D.; Daube, B.; Horowitz, L.; Keene, W.; Heikes, B. Formaldehyde, glyoxal, and methylglyoxal in air and cloudwater at a rural mountain site in central Virginia. *J. Geophys. Res.* **1995**, *100*, 9325−9325.
(22) Berglund, R. N.; Liu, B. Y. H. Generation of monodisperse aerosol standards. *Environ. Sci. Technol.* **1973**, *7*, 147−153.
(23) Pankow, J.; Asher, W. SIMPOL.1: A simple group contribution method for predicting vapor pressures and enthalpies of vaporization of multifunctional organic compounds. *Atmos. Chem. Phys.* **2008**, *8*, 2773−2796.
(24) *Estimation Programs Interface Suite (EPI-Suite) for Microsoft Windows*, version 4.00; Environmental Protection Agency: Washington, DC, 2010 (http://www.epa.gov/oppt/exposure/pubs/episuite.htm).
(25) Joback, K. G.; Reid, R. C. Estimation of pure-component properties from group-contributions. *Chem. Eng. Commun.* **1987**, *57*, 233−243.
(26) Peng, C.; Chan, M. N.; Chan, C. K. The hygroscopic properties of dicarboxylic and multifunctional acids: Measurements and UNIFAC predictions. *Environ. Sci. Technol.* **2001**, *35*, 4495−4501.
(27) Chan, M.; Chan, C. Mass transfer effects in hygroscopic measurements of aerosol particles. *Atmos. Chem. Phys.* **2005**, *5*, 4057−4082.
(28) Sareen, N.; Schwier, A.; Shapiro, E.; Mitroo, D.; McNeill, V. Secondary organic material formed by methylglyoxal in aqueous aerosol mimics. *Atmos. Chem. Phys.* **2010**, *10*, 997−1016.
(29) McNeill, V. F.; Wolfe, G. M.; Thornton, J. A. The oxidation of oleate in submicron aqueous salt aerosols: Evidence of a surface process. *J. Phys. Chem. A* **2007**, *111*, 1073−1083.
(30) Yaws, C. L. *Yaws' Handbook of Thermodynamic and Physical Properties of Chemical Compounds*, Knovel online version; 2003 (http://www.knovel.com).
(31) Loeffler, K. W.; Koehler, C. A.; Paul, N. M.; De Haan, D. O. Oligomer formation in evaporating aqueous glyoxal and methyl glyoxal solutions. *Environ. Sci. Technol.* **2006**, *40*, 6318−6323.
(32) Limbeck, A.; Puxbaum, H.; Otter, L.; Scholes, M. C. Semivolatile behavior of dicarboxylic acids and other polar organic species at a rural background site (Nylsvley, RSA). *Atmos. Environ.* **2001**, *35*, 1853−1862.
(33) Na, K.; Song, C.; Switzer, C.; Cocker, D. R. Effect of ammonia on secondary organic aerosol formation from α-pinene ozonolysis in dry and humid conditions. *Environ. Sci. Technol.* **2007**, *41*, 6096−6102.
(34) Kampf, C. J.; Waxman, E. M.; Slowik, J. G.; Dommen, J.; Pfaffenberger, L.; Praplan, A. P; Prévôt, A. S. H.; Baltensperger, U.; Hoffmann, T.; Volkamer, R. Effective Henry's law partitioning and the salting constant of glyoxal in aerosols containing sulfate. *Environ. Sci. Technol.* **2013**, *47*, 4236−4244.
(35) Nozière, B.; Dziedzic, P.; Córdova, A. Products and kinetics of the liquid-phase reaction of glyoxal catalyzed by ammonium ions (NH_4^+). *J. Phys. Chem. A* **2009**, *113*, 231−237.
(36) Donahue, N. M.; Huff Hartz, K. E.; Chuong, B.; Presto, A. A.; Stanier, C. O.; Rosenhørn, T.; Robinson, A. L.; Pandis, S. N. Critical factors determining the variation in SOA yields from terpene ozonolysis: A combined experimental and computational study. *Faraday Discuss.* **2005**, *130*, 295−309.
(37) Nozière, B.; Dziedzic, P.; Córdova, A. Inorganic ammonium salts and carbonate salts are efficient catalysts for aldol condensation in atmospheric aerosols. *Phys. Chem. Chem. Phys.* **2010**, *12*, 3864−3872.
(38) Chickos, J. S.; Zhao, H. Measurement of the vaporization enthalpy of complex mixtures by correlation-gas chromatography. The vaporization enthalpy of RP-1, JP-7, and JP-8 rocket and jet fuels at T = 298.15 K. *Energy Fuels* **2005**, *19*, 2064−2073.
(39) Turpin, B. J.; Lim, H.-J. Species contributions to PM2.5 mass concentrations: Revisiting common assumptions for estimating organic mass. *Aerosol Sci. Technol.* **2001**, *35*, 602−610.
(40) Windholdz, M. *The Merck Index: An Encyclopedia of Chemicals and Drugs*; Merck & Co.: New York, 1976.
(41) Desboeufs, K.; Losno, R.; Colin, J. Relationship between droplet pH and aerosol dissolution kinetics: Effect of incorporated aerosol particles on droplet pH during cloud processing. *J. Atmos. Chem.* **2003**, *46*, 159−172.
(42) Ervens, B.; Volkamer, R. Glyoxal processing by aerosol multiphase chemistry: Towards a kinetic modeling framework of secondary organic aerosol formation in aqueous particles. *Atmos. Chem. Phys.* **2010**, *10*, 8219−8244.